13th International Symposium on Particle Image Velocimetry – ISPIV 2019
Munich, Germany, July 22-24, 2019

# Experimental assessment of large-scale motions in turbulent boundary layers

**Alejandro Güemes[1]*, Andrea Ianiro[1], Stefano Discetti[1]**

[1] Universidad Carlos III de Madrid, Aerospace Engineering Department, Madrid, Spain

* aguemes@ing.uc3m.es

## Abstract

The effect of high- and low-momentum events on the turbulent statistics of turbulent boundary layers is investigated experimentally. Flow-field measurements are carried out by means of Particle Image Velocimetry (PIV). Turbulence statistics are extracted at high resolution using Ensemble Particle Tracking Velocimetry (EPTV) and a novel technique to increase PIV resolution coupling EPTV with Proper Orthogonal Decomposition (POD). The idea is similar to the EPTV principle, i.e. binning a cloud of vectors to compute POD modes at a resolution higher than that of the standard PIV. Results show a cross-over point in the streamwise Reynolds stresses for the high- and low-momentum events that appears at $y^+ = 3.9\sqrt{Re_\tau} \approx 125$ (with $Re_\tau$ being the friction-based Reynolds number). Moreover, it can be seen that, although their intensity is reduced, the streamwise Reynolds stresses of low-momentum events significantly contribute to the inner peak.

## 1 Introduction

Identifying coherent patterns in turbulent flows and understanding their effects on turbulent dynamics has been of utmost importance for many decades. For what concerns wall-bounded flows, several evidences of these coherent patters, also called large-scale motions (LSMs), are available in several previous studies, such as those carried out by Kline et al. (1967) or Wark and Nagib (1991). These works report the presence of long features of uniform high or low momentum in the logarithmic region of a turbulent boundary layer (TBL). Using a spanwise rake of hot-wires, Hutchins and Marusic (2007a) proved that these elongated regions were extended up to a length of order 20 times the boundary layer thickness $\delta_{99}$. These features were also found experimentally in turbulent pipe and channel flows by Monty et al. (2007).

Understanding of how LSMs affect the region close to the wall is an issue of special relevance. Hutchins and Marusic (2007b) showed that the high- and low-momentum events occurring in the logarithmic region do not only shift the near-wall scales but they also modulate their production, and that this effect becomes stronger for increasing Reynolds numbers. These findings were corroborated by the work of Mathis et al. (2009), which also confirmed the increase of the number of high- and low-momentum events in the logarithmic region with increasing Reynolds numbers. Additionally, Mathis et al. (2009) defined empirically a cross-over point $3.9\sqrt{Re_\tau}$, located at the geometrical center of the logarithmic region. They found that from this cross-over point down to the wall the fluctuating streamwise velocity is more affected by the high-momentum events, while from the cross-over point to the outer region the low-momentum events are dominant. Ganapathisubramani et al. (2012) carried out an experimental campaign to analyze how the large-scale fluctuations modulate the small-scales fluctuations in frequency and amplitude. Apart from finding the same high- and low-momentum effect mentioned previously, they observed that increase of near-wall scales due to high-momentum events is not as strong as the attenuation due to the low-momentum events. While the previous works were focused on the effects of large-scale streamwise fluctuations on small-scale streamwise fluctuations, Talluru et al. (2014) analysed how the large-scale streamwise fluctuations affect the wall-normal, spanwise and shear small-scale fluctuations, showing the same modulation pattern as in streamwise small-scale fluctuations.

The evidence of the effects that LSMs have on the inner scales paves the way towards an active control of wall-bounded turbulent flows based on LSM detection. One of the first works to develop this idea was carried out by Marusic et al. (2010). They proposed a model that predicts the inner-region fluctuations based on how the large-scale fluctuations at the geometrical center of the logarithmic region amplify and modulate the theoretical inner-wall fluctuations in the absence of any large-scale footprint or modulation. Mathis et al. (2011) provided a deeper explanation on how the prediction model works, and they tested it in zero-pressure-gradient TBL, channels, pipes and TBLs with adverse pressure gradient. Their results showed a good agreement between measurements and predictions in the inner layer, and they were even able to capture the evolution with the Reynolds number. It is worth to say that their results encourage the idea that the theoretical inner-wall fluctuations in the absence of any large-scale footprint or modulation are universal for wall-bounded flows. Based on the model by Marusic et al. (2010), Mathis et al. (2013) developed a model to estimate wall-shear-stress fluctuations using LSMs information. The model was shown to provide good prediction results, and to catch reasonably well the Reynolds-number dependence of the wall-shear-stress fluctuation magnitude showed earlier by Örlü and Schlatter (2011). Additionally, a theoretical formulation of the predictive model allowed the authors to identify that the amplitude and frequency modulation coefficients should be the same for this model, resulting in a reduction of the parametric space.

It has to be noted that in the previous mentioned works the effect of high- and low-momentum events on the turbulent statistics was analyzed using one-point measurements. The analysis of flow fields by means of particle image velocimetry (PIV) allows to identify LSMs via "global events", using for instance proper orthogonal decomposition (POD) as in the works by Wu (2014) and Discetti et al. (2019). In the present article, the effects of high- and low-momentum events on the turbulence statistics are investigated using ensemble-particle tracking velocimetry (EPTV) as in Agüera et al. (2016). The high- and low-momentum events are identified using POD. With this objective, an experimental campaign has been carried out to acquire date from a TBL developing on a flat plate in a subsonic wind tunnel. PIV has been used to extract flow fields for subsequent modal analysis with POD. To compute the turbulence statistics, four data sets have been defined: the full set of PIV images, PIV images containing high-momentum events, PIV images containing low-momentum events, and PIV without the contribution of LSMs. Turbulent statistics has been obtained at high resolution with EPTV approach, thus obtaining a combination of a large field of view and high level of detail in the statistics. The article is organised as follows: Section 2 reports a description of the experimental apparatus, together with the strategies used to post-process the acquired data. The methodology based on the modal analysis of the instantaneous flow fields that has been used to identify the LSMs and to compute their turbulence statistics at several positions downstream of the rib is presented in Section 3. Finally, the analysis results are presented in Section 4, prior to presenting the conclusions of this work in Section 5.

## 2 Experimental Set-Up

The experimental campaign has been carried out in the Göttingen-type wind tunnel of the Aerospace Engineering Group at Universidad Carlos III de Madrid. The test section is 1.5 m long with a cross-sectional area of $0.4 \times 0.4$ m$^2$. The wind tunnel speed ranges from 4 m/s to 20 m/s, showing a freestream turbulence intensity below 1%.

A turbulent boundary layer develops on a smooth methacrylate flat plate of 1.25 m length and 10 mm thickness, spanning the entire height of the wind tunnel and located 0.09 m far from the closer wind tunnel wall. Throughout this article the $x$, $y$, and $z$ are streamwise, wall-normal, and spanwise directions respectively. The mean streamwise, wall-normal, and spanwise velocities are referred to as $U$, $V$, and $W$ respectively, while $u$, $v$, and $w$ are the streamwise, wall-normal, and spanwise velocity fluctuations. The leading edge of the flat plate follows the shape of an ellipse with aspect ratio 5. Moreover, the trailing edge is equipped with a 0.15 m long flap in order to modify the position of the stagnation point. In order to stimulate the transition of the boundary layer to the turbulent regime, a tripping device has been used. The tripping device is composed by a 2.4 mm-high turbulator in combination with two DYMO tapes (with the embedded letter V pointing in the flow direction and a nominal height of 0.3 mm). The tripping device has been located at $x = 0.05$ m. The procedure presented by Sanmiguel Vila et al. (2017) has been followed to ensure that TBL is not affected by tripping effect. A sketch of the experimental set-up used in the present experimental campaign is presented in Figure 1.

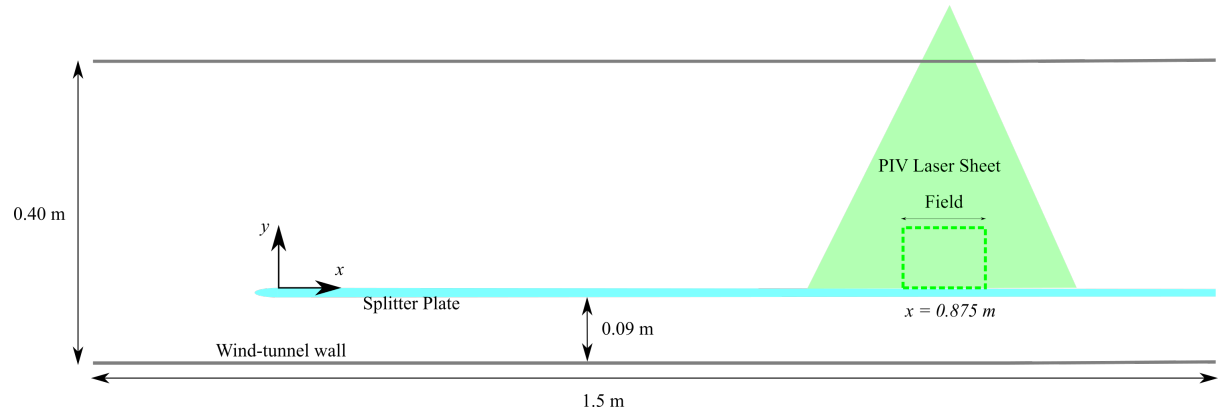


Figure 1: Top view sketch of the experimental setup. The flat plate is mounted over the non-modified lateral wall by means of bars.

To verify that the TBL corresponds to a ZPG case, the flat plate has been equipped with pressure taps to get insight of the pressure distribution along it. The first tap has been located at $x = 0.025$ m, and the following taps have been separated by 0.05 m of distance. Additionally, the taps have been shifted in the spanwise direction from the streamwise centerline 0.025 m to the top and to the bottom alternatively. Using these pressure taps, the pressure distribution has been characterized in terms of the pressure coefficient $C_p$, which is defined for an incompressible flow as:

$$C_p = \frac{P - P_{ref}}{1/2\rho U_{ref}^2} = 1 - \left(\frac{U_\infty}{U_{ref}}\right)^2, \tag{1}$$

where $P$ is the local static pressure, $P_{ref}$ is the static pressure measured at $x = 0.025$ m, $U_\infty$ is the local free-stream velocity and $U_{ref}$ is the reference free-stream velocity at $x = 0.025$ m. It has to be remarked that a nearly-zero pressure gradient has been achieved with very good approximation, with $C_p$ values between $-0.025$ and 0.025 in the measurement region.

PIV has been used to obtain velocity fields. A total of 39000 particle image pairs were acquired. PIV raw images were obtained imaging a plane parallel to the freestream, normal to the flat plate, with the illumination region starting at the streamwise location $x = 0.875$ m. The flow has been seeded using a Laskin nozzle that generates droplets of Di-Ethyl-Hexyl-Sebacate (DEHS) with 1 m diameter. The seeded flow has been illuminated by means of a light sheet produced by a dual cavity Ng:Yag Quantel Evergreen laser (200 mJ/pulse at 10 Hz). An ANDOR Zyla sCMOS 5.5 MP camera (2560 $\times$ 2160 pixel array, 6.5 $\times$ 6.5 $\mu$m pixel size) has been used to capture PIV images, with a resolution about 48500 pix/m. The camera is equipped with a Tokina 100 mm lens. The lens aperture is set to $f_\# = 16$ and the objective is set slightly out of focus in order to artificially increase the particle image size and avoid peak locking. The camera and the laser triggers are coordinated by means of Quantum composer 9520 Series Pulse Delay Generator. Laser reflections and illumination background have been removed in order to improve the image quality by using the POD-based approach proposed by Mendez et al. (2017).

The post-processing of PIV images has been carried out using a code developed at University of Naples Federico II. This code applies the iterative multi-grid/multi-pass algorithms proposed by Willert and Gharib (1991) and Soria (1996) and the image deformation algorithm proposed by Scarano (2001) as interrogation strategy, with final interrogation windows of 32 $\times$ 32 pixels with 75% overlap. To improve the accuracy of the code, a B-Spline interpolation has been used in the iterative procedure, as proposed by Astarita and Cardone (2005) and Astarita (2006).

# 3 Methodology

The procedure to identify high- and low-momentum events, and to extract high-resolution statistics, is outlined in this section. Proper Orthogonal Decomposition (POD) identifies orthonormal basis functions to decompose the velocity fluctuations. The basis functions are sorted according to their contribution to the turbulent kinetic energy. In the *snapshot POD* implementation, the velocity fields are rearranged is a snapshot matrix $\underline{\underline{U}}$ of size $n_t \times n_p$, where $n_t$ is the number of PIV snapshots and $n_p$ is the number of pixel in the images. The snapshot matrix is then decomposed via Singular Value Decomposition. The temporal coefficients are the columns of the matrix $\underline{\underline{\Psi}}$, while the spatial modes are the columns of $\underline{\underline{\Phi}}$. The matrix $\underline{\underline{\Sigma}}$ contains on its diagonal the square root of the integral turbulent kinetic energy corresponding to each mode.

$$\underline{\underline{U}} = \underline{\underline{\Psi}}\,\underline{\underline{\Sigma}}\,\underline{\underline{\Phi}} \tag{2}$$

The time coefficients of the first POD mode are used to identify high- and low-momentum events. The first POD mode corresponds to those structures present in the flow field with larger energy, i.e. the high- and low-momentum large-scale events, as showed by Wu (2014). The criterion is based on the value of the time coefficients from the first mode: snapshots with first-mode time coefficient value larger than one standard deviation of the first-mode time coefficient correspond to low- or high-momentum events, depending on the sign. It has to be noted that sign criteria of Eq.3 depends on the spatial configuration of the flow structure of the first POD spatial mode. In case the first mode corresponds to a high-momentum event, all the snapshots for which the first-mode time coefficient $\psi_1$ is larger than one standard deviation correspond to high-momentum events. Given that temporal modes have unitary euclidean norm, this criterion can be formalized as:

$$\text{Flow field} \equiv \begin{cases} \text{high-momentum event}, & \text{if } \psi_1 > \frac{1}{\sqrt{n_t}} \\ \text{low-momentum event}, & \text{if } \psi_1 < -\frac{1}{\sqrt{n_t}} \\ \text{no extreme event}, & \text{otherwise} \end{cases} \tag{3}$$

After applying thresholding, the turbulence statistics for the high- and low-momentum event subsets are computed. The baseline case (i.e. statistics on the overall dataset) is analyzed using a polynomial-fit-based Ensemble Particle Tracking Velocimetry (Agüera et al., 2016) to reduce the effect of limited spatial resolution (Kähler et al., 2012). To overcome this problem, EPTV has been used. The bins used for averaging have a size of $400 \times 2$ pixels. The same approach can be applied directly also on the subsets containing high- and low-momentum events, according to the criterion of Eq. 3.

Additionally, it is desirable to compare the high- and low-momentum turbulence statistics with the turbulence statistics without extreme events contribution, i.e. filtering out the contribution of the first POD mode. This requires computing the first spatial mode with the same resolution of the EPTV, and then subtract its contribution to the snapshots of the dataset. To this purpose, a mixed approach between EPTV and POD is proposed. The time coefficients obtained from the decomposition of the snapshot matrix built with the PIV data are used as a temporal basis to carry out this operation. Extended POD modes of the EPTV flow fields are computed followint Eq. 4. In particular the modes are obtained as the average of the particles displacements contained in the bins used for the Ensemble PTV, each particle displacement being multiplied by the corresponding time coefficient of the relative snapshot:

$$\sigma_i \phi_i = \sum_{t=1}^{n_t} \frac{1}{A_{bin}} \int_{A_{bin}} \psi_{t,i_{PIV}} u_{t_{EPTV}} dx \tag{4}$$

Subsequently, the contribution of each EPTV mode to the streamwise energy fluctuation is:

$$\overline{uu}_i^* = \frac{(\sigma_i \phi_i)^2}{n_t} \tag{5}$$

In order to obtain turbulent statistics without LSM contribution, the final step is to subtract the contribution of the first mode from the streamwise fluctuations. This approach can be also followed for wall-normal and shear fluctuations.

$$\overline{uu}_{NS} = \overline{uu}_{EPTV} - \overline{uu}_1^* \tag{6}$$

# 4 Results

The boundary layer parameters are reported in Table 1. These quantities are the free-stream velocity $U_\infty$, the wall-friction velocity $u_\tau$, the boundary-layer thickness $\delta_{99}$, the displacement thickness $\delta^*$, the Reynolds numbers $Re_\tau$ and $Re_\theta$ (based on wall friction velocity $u_\tau$, and momentum thickness $\theta$ respectively), and the shape factor $H_{12}$. In this work, the absolute wall position and the friction velocity have been computed using the composite profile proposed by Chauhan et al. (2009), which has been showed to be able to produce robust results if near-wall measurements are available (Örlü et al. (2010); Rodríguez-López et al. (2015); Vinuesa and Nagib (2016)). EPTV measurements provide a sufficiently large number of points within the sublayer and buffer region in order to correct for the absolute wall position and determine the friction velocity without relying on log-law constants.

| $U_\infty$ [m/s] | $u_\tau$[m/s] | $\delta_{99}$ [mm] | $\delta^*$ [mm] | $Re_\tau$ | $Re_\theta$ | $H_{12}$ |
|---|---|---|---|---|---|---|
| 15.5 | 0.64 | 24.7 | 3.7 | 1040 | 2800 | 1.36 |

Table 1: Experimental parameters for the boundary layer profile in the present article. The measurement station is located at x = 0.875 m.

Turbulent statistics profiles are presented in Fig. 1, where the color code stands for normal TBL (—), high-momentum event TBL (—), and low-momentum event TBL (—). The inner scaling is based on the friction velocity estimated from the baseline case. The mean velocity profiles, reported in Fig. 1a), outline that low-momentum events have a larger wake and have a lower mean value, while the high-momentum events show the opposite effect. Fig. 1b) shows the streamwise Reynolds stress profiles. It can be seen that the high-momentum events, which are regions of flow with positive fluctuations going towards the wall (also known as sweeps), have a larger influence closer to the wall, being decreased when going away form the wall. In the opposite way, the low-momentum events, which are regions of flow with negative fluctuations convected away from the wall (also known as ejections), weakly contribute to the inner peak while contribute significantly to the turbulent fluctuations in the wake of the TBL. This behaviour leads to the conclusion that the attenuation of near-wall scales due to low-momentum events is stronger than the increase due to high-momentum events, as shown by Ganapathisubramani et al. (2012). Looking how high-and low-momentum events interact between them it is found a cross-over point that appears at $y^+ = 3.9\sqrt{Re_\tau} \approx 125$. This cross-over point is consistent with the cross-over location in the amplitude modulation coefficient found by Mathis et al. (2009), and also shown by Ganapathisubramani et al. (2012). This finding is quite interesting, because in those previous works the cross-over point was defined empirically based on the wavelength of temporal signal in fixed positions, using it as a cut-off frequency between high- and low-momentum events. On the other hand, our work uses a "global" criterion to perform a discrimination between high- and low-momentum events, i.e. it exploits the spatial information.

When analyzing how Reynolds wall-normal and shear stresses are affected by high- and low-momentum events it can be found the same cross-over point as in the streamwise stress, thus corroborating the findings of Talluru et al. (2014). For what concerns the wall-normal stress the effect of high-momentum events is larger close to the wall, while the low-momentum events have more incidence far from the wall. This is indicative of the regions where each of the events lives. However, when comparing the high- and low-momentum events with the wall-normal stresses without LSM contribution, it is found that low-momentum events do not produce an attenuation of the wall-normal stress but a change in its distribution. In the Reynolds shear stress, apart from the cross-over point, it can be found the opposite effect as in the streamwise stress: while the low-momentum events have a large contribution to the Reynolds shear stress, the high-momentum events result in a shear stress profile similar to that of the TBL without the contribution of the first mode.

With respect to the contribution of first POD mode to the turbulent statistics, it can be seen that high- and low momentum events have a constant incidence in the streamwise stress along the wall normal direction, while their incidence on the wall-normal stress is larger in the logarithmic region than in the inner region or

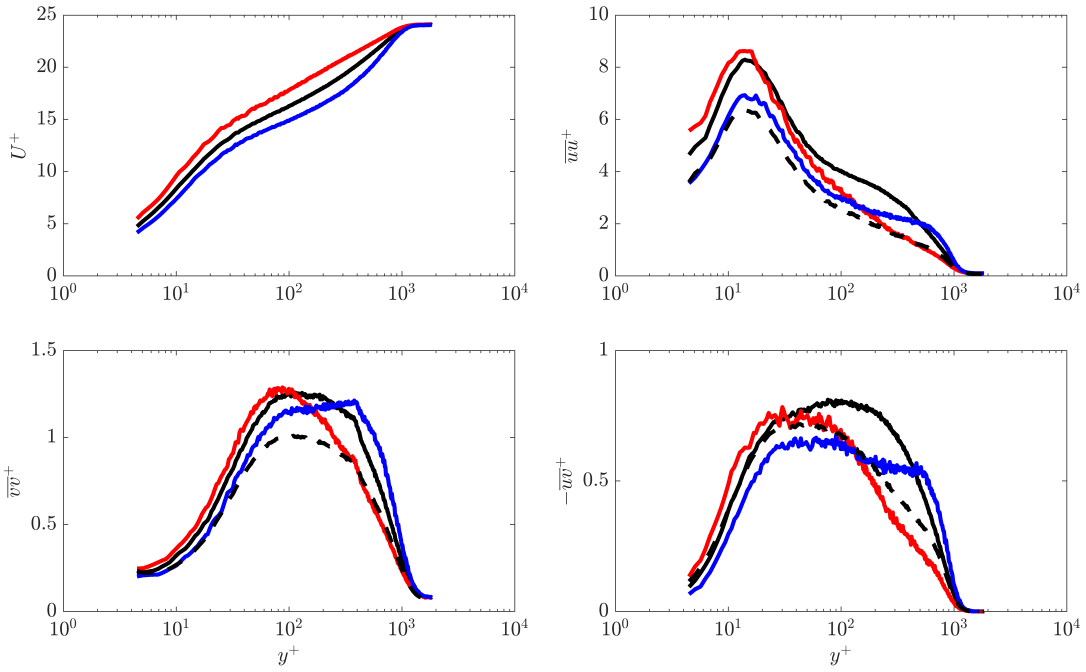


Figure 2: Inner-scaled turbulent statistics for TBL (——), TBL without first mode contribution (– –), high-momentum event TBL (——), and low-momentum event TBL (——). Plots refers to: a) mean streamwise velocity, b) streamwise Reynolds stress, c) wall-normal Reynolds stress and d) Reynolds shear stress.

the wake of the TBL. Regarding the Reynolds shear stress, it can be seen that large part of the first mode contribution lies in the logarithmic and outer parts of the TBL, where turbulence is produced.

## 5 Conclusion

In this work the effect of LSMs on the turbulent statistics has been investigated using high-resolution flow fields. To discriminate between high- and low- momentum events, the temporal coefficient of the first POD mode has been used. This method, although still empirical, differs significantly from using wavelengths in one-point temporal signals as cut-off between high- and low-momentum events. The information collected from two-dimensional flow fields has more relevance to the LSMs, which are spatial structures, than the information collected from one-point measurements. However, it has to be taken into account that LSMs have a streamwise dimension larger than our acquisition field, thus making difficult a full understanding on how they affect the turbulence statistics.

Apart from studying the effect of LSMs on the turbulent statistics, this work proposes a method to decompose the EPTV turbulent statistics into their POD modes contribution. The method allows to obtain POD modes with high resolution, with a principle similar to that used by EPTV to extract high-resolution turbulent statistics.

Regarding the results, it is worth mentioning that the same cross-over point at $y^+ \approx 3.9\sqrt{Re_\tau}$ between high- and low-momentum events showed, among others, by Mathis et al. (2009) and Ganapathisubramani et al. (2012) is found, although the method to detect the events is different. It is shown that high-momentum events have a larger contribution to the inner peak of the streamwise stress, while the low-momentum events produce a large attenuation. This dominance of the high-momentum events is shown to be inverted in the outer part of the TBL, where low-momentum events become dominant.

## Acknowledgements

This work has been partially supported by grant DPI2016-79401-R funded by the Spanish State Research Agency (SRA) and European Regional Development Fund (ERDF).

## References

Agüera N, Cafiero G, Astarita T, and Discetti S (2016) Ensemble 3D PTV for high resolution turbulent statistics. *Meas Sci Technol* 27:124011

Astarita T (2006) Analysis of interpolation schemes for image deformation methods in PIV: effect of noise on the accuracy and spatial resolution. *Exp Fluids* 40:977–987

Astarita T and Cardone G (2005) Analysis of interpolation schemes for image deformation methods in PIV. *Exp Fluids* 38:233–243

Chauhan KA, Monkewitz PA, and Nagib HM (2009) Criteria for assessing experiments in zero pressure gradient boundary layers. *Fluid Dyn Res* 41:021404

Discetti S, Bellani G, Örlü R, Serpieri J, Vila CS, Raiola M, Zheng X, Mascotelli L, Talamelli A, and Ianiro A (2019) Characterization of very-large-scale motions in high-re pipe flows. *Experimental Thermal and Fluid Science* 104:1–8

Ganapathisubramani B, Hutchins N, Monty J, Chung D, and Marusic I (2012) Amplitude and frequency modulation in wall turbulence. *J Fluid Mech* 712:61–91

Hutchins N and Marusic I (2007a) Evidence of very long meandering features in the logarithmic region of turbulent boundary layers. *J Fluid Mech* 579:1–28

Hutchins N and Marusic I (2007b) Large-scale influences in near-wall turbulence. *Philosophical Transactions of the Royal Society A: Mathematical, Physical and Engineering Sciences* 365:647–664

Kähler CJ, Scharnowski S, and Cierpka C (2012) On the resolution limit of digital particle image velocimetry. *Exp Fluids* 52:1629–1639

Kline SJ, Reynolds WC, Schraub F, and Runstadler P (1967) The structure of turbulent boundary layers. *J Fluid Mech* 30:741–773

Marusic I, Mathis R, and Hutchins N (2010) Predictive model for wall-bounded turbulent flow. *Science* 329:193–196

Mathis R, Hutchins N, and Marusic I (2009) Large-scale amplitude modulation of the small-scale structures in turbulent boundary layers. *J Fluid Mech* 628:311–337

Mathis R, Hutchins N, and Marusic I (2011) A predictive inner–outer model for streamwise turbulence statistics in wall-bounded flows. *J Fluid Mech* 681:537–566

Mathis R, Marusic I, Chernyshenko SI, and Hutchins N (2013) Estimating wall-shear-stress fluctuations given an outer region input. *J Fluid Mech* 715:163–180

Mendez M, Raiola M, Masullo A, Discetti S, Ianiro A, Theunissen R, and Buchlin JM (2017) POD-based background removal for particle image velocimetry. *Exp Thermal Fluid Sci* 80:181–192

Monty J, Stewart J, Williams R, and Chong M (2007) Large-scale features in turbulent pipe and channel flows. *J Fluid Mech* 589:147–156

Örlü R, Fransson JHM, and Alfredsson PH (2010) On near wall measurements of wall bounded flows – the necessity of an accurate determination of the wall position. *Prog Aero Sci* 46:353–387

Örlü R and Schlatter P (2011) On the fluctuating wall-shear stress in zero pressure-gradient turbulent boundary layer flows. *Phys fluids* 23:021704

Rodríguez-López E, Bruce PJK, and Buxton ORH (2015) A robust post-processing method to determine skin friction in turbulent boundary layers from the velocity profile. *Exp Fluids* 56:68

Sanmiguel Vila C, Vinuesa R, Discetti S, Ianiro A, Schlatter P, and Örlü R (2017) On the identification of well-behaved turbulent boundary layers. *J Fluid Mech* 822:109–138

Scarano F (2001) Iterative image deformation methods in piv. *Meas Sci Technol* 13:R1

Soria J (1996) An investigation of the near wake of a circular cylinder using a video-based digital cross-correlation particle image velocimetry technique. *Exp Thermal Fluid Sci* 12:221–233

Talluru K, Baidya R, Hutchins N, and Marusic I (2014) Amplitude modulation of all three velocity components in turbulent boundary layers. *J Fluid Mech* 746

Vinuesa R and Nagib HM (2016) Enhancing the accuracy of measurement techniques in high Reynolds number turbulent boundary layers for more representative comparison to their canonical representations. *European Journal of Mechanics-B/Fluids* 55:300–312

Wark CE and Nagib H (1991) Experimental investigation of coherent structures in turbulent boundary layers. *J Fluid Mech* 230:183–208

Willert CE and Gharib M (1991) Digital particle image velocimetry. *Exp Fluids* 10:181–193

Wu Y (2014) A study of energetic large-scale structures in turbulent boundary layer. *Phys Fluids* 26:045113